International Journal of Bioprinting

SHORT COMMUNICATION

# Development and characterization of an automated active mixing platform for hydrogel bioink preparation

**Jiannan Li[1†], Tara Shelby[1†], Hossein Vahid Alizadeh[1], Hannah Shelby[1], Yunzhi Peter Yang[1,2,3*]**

[1]Department of Orthopedic Surgery, Stanford University, 240 Pasteur Drive, Stanford, CA94304, USA

[2]Department of Materials Science and Engineering, Stanford University, 496 Lomita Mall, Stanford, CA94305, USA

[3]Department of Bioengineering, Stanford University, 443 Via Ortega, Stanford, CA94305, USA

## Abstract

Bioink preparation is an important yet challenging step for bioprinting with hydrogels, as it involves fast and homogeneous mixing of various viscous components. In this study, we have developed an automated active mixing platform (AAMP), which allows for high-quality preparation of hydrogel bioinks. The design of AAMP, adapted from syringe pumps, provides many advantages, including low cost, automated control, high precision, customizability, and great cytocompatibility, as well as the potential to intelligently detect the homogeneity. To demonstrate the capability of AAMP, mixing of different hydrogel components, including alginate and xanthan gum with and without $Ca^{2+}$, alginate and Laponite, PEGDMA and xanthan gum, was performed to investigate an alginate hydrogel preparation process. Colorimetric analyses were carried out to evaluate the mixing outcome with AAMP. Result showed that AAMP can prepare homogeneous hydrogel mixing in a fast and automated fashion. A multiphysics COMSOL simulation is carried out to further validate the results. Moreover, cell viability and proliferation study were performed in a cell encapsulation mixing experiment to validate the cytocompatibility of the AAMP. The AAMP has demonstrated great capability in hydrogel bioink preparation and could therefore holds great promise and wide applications in bioprinting and tissue engineering.

***Keywords:*** Bioprinting; Hydrogel; Tissue engineering; Bioink; Biomaterials

[†]These authors contributed equally to this work.

***Corresponding authors:**
Yunzhi Peter Yang
(ypyang@stanford.edu)

**Citation:** Li J, Shelby T, Alizadeh HV, *et al.*, 2023, Development and characterization of an automated active mixing platform for hydrogel bioink preparation. *Int J Bioprint*.
https://doi.org/10.18063/ijb.705

**Received:** May 03, 2022

**Accepted:** September 27, 2022

**Published Online:** March 10, 2023



## 1. Introduction

Hydrogels, as an essential class of materials, are becoming increasingly common in many fields, including tissue engineering, pharmaceutics, and wound dressings[1]. Specifically, they are becoming prevalent in the field of tissue engineering, acting as scaffold materials that provide desired mechanical properties and biological functionalities[2-4]. With the advancement of additive manufacturing, particularly three-dimensional (3D) printing, hydrogels have gained increasing interest as bioinks for the printing of tissue engineered scaffolds[5-14].

Despite tremendous breakthroughs made in hydrogel bioprinting, challenges remain, with achievement of hydrogel bioink homogeneity being one of them. Syringe extrusion is the most used hydrogel bioprinting approach, where the hydrogel is first prepared by mixing of the monomer, crosslinker, and other additives, and then incubated to form the hydrogel, followed by the loading of hydrogel into a syringe for subsequent printing[15]. During this process, homogeneous mixing and proper loading are crucial to the homogeneity of the final product to be printed[16]. As the hydrogel pre-polymer solutions are usually highly viscous[17] and difficult to mix, traditional vortexing usually works poorly for hydrogel pre-polymer mixing. The fast gelation kinetics also result in the change of viscosity and diffusion coefficients during the mixing, which adds more complexity to the mixing process[15]. Moreover, during all the mixing and loading steps, it is difficult to avoid formation or trapping of air bubbles[15]. These factors can greatly hinder the bioink preparation process, resulting in heterogeneous bioink, which, in turn, affects the print quality.

Various efforts have then emerged to address these issues so as to achieve a homogeneous bioink. The most straightforward approach is to apply powerful mixing apparatus. Different types of mixing apparatus, including blenders[18,19] or agitators,[20,21] can be used. These powerful mixers can achieve fast mixing homogeneity even before the sol-gel transition begins, so the change in viscosity and diffusivity can be negligible. They are also capable of batch-processing large quantity of gels due to their large form factors. However, these methods are still subject to formation or trapping of air bubbles during the blending or on the loading of bioink into the printing syringe barrel. Once the gel is formed, it is relatively difficult to be transferred from one container to another without trapping air. To address this, approaches have been developed to perform the mixing in the format of syringes. For example, a static syringe mixer was developed with the brandmark of CELL-MIXER[22-24]. In such static mixer, different components to be mixed are loaded in separate syringes placed in parallel and pushed together through a mixing tip whose outlet is connected to the target syringe. The mixing tip is designed with swirling blades, so that the components can be thoroughly mixed when passing through. As the mixer is static and the mixing is a one-time operation, the homogeneity of the mixing depends on the length and geometry of the mixing tip. For very viscous components, the tip might never be long enough to achieve homogeneous mixing.

In these cases, another type of syringe-based mixer, referred to as active mixer herein, would be preferred. In an active mixer, two syringes loaded with hydrogel components are placed against each other and connected by a female-to-female syringe connector. By pumping the two-syringe system back and forth, the components would start mixing in the sealed chamber formed by the two syringes and the connector[25]. As the back-and-forth pumping could have infinite number of cycles, homogeneity could eventually be reached if the components are non-reacting. However, the gelation of hydrogel pre-polymer components adds more complexity to the process, and if not mixed fast enough, gelation would affect the final homogeneity. Therefore, the pumping is expected to be fast with high pumping frequency and pumping speed. So far, this approach is still carried out by manually pumping the two syringes, which is not only laborious, but also limited in its pumping speed and frequency. With the pumping of very viscous fluids repeatedly with only thumbs in the span of a few minutes, one may even be at risk for long-term ergonomics-based diseases. Moreover, manual operation induces human error as the pumping speed can hardly be kept constant. All these factors add up to the complexity of the mixing and gelation process during the hydrogel bioink preparation, making it difficult to analyze and standardize. Therefore, many hydrogel preparation approaches still suffer from batch-to-batch variations[26,27]. Such variation not only limits the applications of hydrogel bioinks, but also hinders the theoretical understanding of the intrinsic gelation process of hydrogels.

In this work, we propose an automated active mixing platform (AAMP). The AAMP is an active mixer that has the potential to relieve this variation obstacle. On one hand, the AAMP frees human labor from the laborious pumping operation. On the other hand, it allows for controllable mixing settings, including pumping cycles and speed. Such capabilities can help minimize the batch-to-batch variation of hydrogel bioinks, as was validated by consecutive successful rounds of homogenous mixing. We also systematically characterized the AAMP performance under different parameter settings, including cycle and speed, using a representative alginate/$Ca^{2+}$ hydrogel with high-viscosity additives. All experiments were validated using colorimetric analysis[25]. We believe, the high repeatability provided by AAMP could greatly facilitate the fabrication of hydrogel bioink with high quality, as well as provide more predictable data for theoretical study of the gelation process. Furthermore, to validate our experimental results and provide more insights into the hydrogel gelation study, we also carried out COMSOL simulation for the AAMP mixing process. We varied mixing cycle and speed in the simulation and the outcome matched with experimental results. In addition,

assessment of cell viability and proliferation ability post-mixing was conducted, as both measures are essential for the AAMP-mixed bioinks to be effectively used in tissue engineering. Together, the experimental and simulation results provided instructive information on how to achieve high-quality hydrogel bioink with homogeneity. Beyond being a viable option in terms of its efficacy, our design with chassis size can be extended/reduced and movable stop sensors allow for a "one-size-fits-all approach", in which the AAMP can accommodate various syringe lengths and mixing volumes. For all these reasons, we believe that the AAMP holds great promise in hydrogel bioprinting and tissue engineering.

## 2. Materials and methods

### 2.1. Design and set-up of the device

The AAMP is composed of a chassis, two pushing blocks, two holding blocks, a stepper motor (Nema 17) with a TB6600 (Toshiba) driver and 24V power supply (Figure 1). A 1/4"-20 lead screw is connected to the stepper motor for linear motion. All structural components were designed in Solidworks and 3D printed (Dremel) with polylactic acid (PLA). During operation, the holding blocks held the syringe barrels in place, while the pushing blocks, attached to the motor through a common lead screw, moved the syringe pistons back and forth, creating the cyclic pumping motion. The movement was programmed and controlled by an Arduino Uno. Both the TB6600 motor controller and the 24 V power supply were specifically chosen to allow for a speed sufficient for both adequate mixing and overcoming the pressures inside the syringe. The baseline speed used in the following experiments, unless stated otherwise, is 3000 rpm. Added on either side of the chassis was proximity sensors (Gikfun MC-38 wired door sensor magnetic switches for Arduino) for limiting the range of motion of the pushing blocks. A pair of 10-mL syringes (inner diameter 14.4 mm) was inserted into the device and connected through a female-female syringe connector (inner diameter 4.3 mm). While a volume of 10 mL was chosen, syringes of larger and smaller volumes can be loaded and inserted as well.

### 2.2. Preparation of alginate hydrogel for characterization

About 2.5% of sodium alginate (high molecular weight; Sigma-Aldrich, MO, USA) was first prepared in deionized water with red food dye. About 6% of xanthan gum (Sigma-Aldrich, MO, USA) solution was then prepared in deionized water separately with blue food dye and 2 mg/mL $CaSO_4$ slurry (Sigma-Aldrich, MO, USA). The two separate solutions were then vortexed and left overnight to reach homogeneity. Then, the two solutions were centrifuged at 3000 rpm for 4 min to remove air bubble. A volume of 1.5 mL of each of the solutions was then loaded into the 10-mL syringes, and mixed at 1:1 ratio using AAMP. In the colorimetric test, 2.5% of sodium alginate and 6% of Laponite (BYK, USA), or 20% polyethylene glycol dimethacrylate (PEGDMA; molecular weight = 1000) and 6% of xanthan gum were also used for mixing outcome evaluation with red and blue dyes, respectively.

### 2.3. Rheological characterization

2.5% of sodium alginate and 6% of xanthan gum solution were prepared separately. Their viscosities were measured using flow ramp tests with an ARES-G2 rheometer (TA Instruments, DE, USA). For the flow ramp test, the shear rate was gradually increased from 0 to 100 1/s, while the stress and viscosity were recorded and plotted. Moreover, to study the effect of gelation on viscosity, the two solutions were mixed thoroughly, and the viscosity of the mixture was continuously monitored for 10 min under a shear rate of 10 1/s.

### 2.4. Characterization of hydrogel mixing

After mixing, the homogeneity of the hydrogel was analyzed by colorimetry method. Our analysis includes comparison of hydrogel with and without the alginate/$Ca^{2+}$ reaction, differing mixing cycles (5, 10, 20, 30, and 50) and differing speeds (750 rpm, 1500 rpm, and 3000 rpm) of the same mixing cycles. The speeds of 750 rpm, 1500 rpm, and 3000 rpm correlate to theoretical linear speeds of 952.5 mm/min, 1905 mm/min, and 3180 mm/min. After mixing, the dye-containing gel mixture was extruded and sandwiched between two glass sides separated by SecureSeal™ imaging spacers. Pictures of the gel mixture

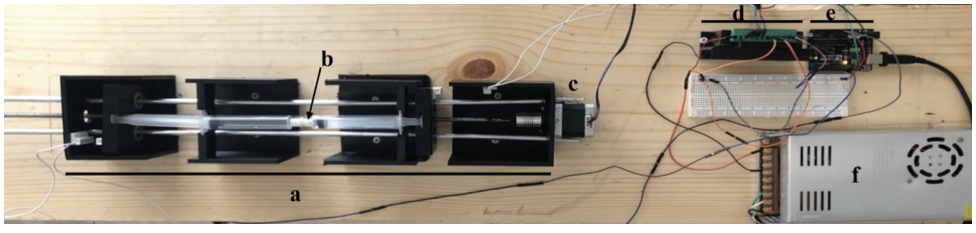


**Figure 1.** Top view of the automated dual-syringe mixing device with (a) device body, (b) syringe-syringe female connecter, (c) NEMA 17 motor, (d) TB6600 motor controller, (e) Arduino Uno, and (f) 24V power supply.

were then taken, followed by measuring their red (R) and blue (B) values in RGB fashion at 40 randomly sampled pixels using image processing software (MATLab). The standard deviation or percent variance of R and B values was then calculated as an indication of the homogeneity.

### 2.5. Multiphysics modeling and simulation with COMSOL

COMSOL Multiphysics simulation software was used to simulate the mixing process in the AAMP at a frequency of 1 Hz for up to 50 cycles. Geometry of the dual-syringe compartment was directly reconstructed in COMSOL. Using moving walls together with a moving mesh, back and forth motion was coupled with fluid dynamics (CFD) model to allow for comparison to the experimental data. Viscosities of the fluid components were substituted based on experimental value from the rheological measurement. Time response of fluid velocity, pressure, and concentrations were plotted at selected time points after the computation.

### 2.6. Cell viability study

A 4-day cell viability study was performed by mixing cell-laden hydrogel components with AAMP. Human mesenchymal stem cells (hMSCs) were cultured in DMEM medium (Life Technologies, USA) supplemented with 10% of fetal bovine serum (FBS, Life Technologies, USA) and 1% of penicillin and streptomycin. For encapsulation of cells in the hydrogel, hMSCs were trypsinized and added to 2.5% alginate solution before mixing at 1:1 ratio with 6% of xanthan gum. For dissolving alginate and xanthan gum, DMEM medium was used as the solvent instead of deionized water. After 10, 30, and 50 cycles of mixing in AAMP, hydrogels were extruded into a mold, forming discs with a diameter of 6 mm and a thickness of 0.45 mm. After physical crosslinking by submerging in 1% of $CaCl_2$ solution for 1 min, samples were then transferred into a 24-well plate, with 1 mL DMEM medium added to each well for culturing. Samples were then analyzed on days 0, 1, and 4. On analyzing, samples were washed with medium. Live/dead staining kit (Invitrogen™, Thermo Fisher, Waltham, MA) was used to visualize live and dead cells. Results were obtained with a fluorescence microscope (Zeiss, Germany) and the viability was analyzed through MATLab scripts by counting live and dead cells using image analysis.

### 2.7. Cell proliferation

Four-week cell proliferation was evaluated by DNA quantification. Similar to the viability experiment, hMSC – or human umbilical vascular endothelial cell (HUVEC) – encapsulated hydrogels were molded into discs with 6 mm diameter and 0.45 mm thickness. After crosslinking, hMSC- and HUVEC-laden samples were cultured in DMEM and HUVEC growth medium, respectively, and collected on days 0, 3, 7, 14, 21, and 28. At each time point, samples were collected into 1.5-mL centrifuge tubes and mechanically broken down with polypropylene pestles (Bio Plas, CA, USA) in 500 µL of 1% of Triton solution in PBS. The resulted solution was then sonicated to lyse the cell membrane. The amount of DNA was then measured with PicoGreen dsDNA assay kit (Invitrogen, MA, USA).

## 3. Results and discussion

### 3.1. AAMP system setup

Figure 1 shows the AAMP from the top view, including the structural set-up and control electronics. The overall device is lightweight and portable, establishing it as an efficient and low-cost option compared to that which exists on the market today. The chassis sits on two rods that allow for size manipulation of the device's body. The AAMP is controlled by Arduino which is easily customizable for speed and cycle settings. The stop sensors are located on the side walls of the chassis and are adjustable, allowing the user to regulate how far each syringe is pushed. This setting is especially important for the "one-size-fits-all" approach, in which our AAMP system is able to accommodate syringes of different sizes and varying mixing volumes.

### 3.2. Colorimetric characterization of AAMP

We have carried out characterization for the AAMP to study the effect of different mixing conditions on the mixing outcome. We first mixed 2.5% of sodium alginate and 6% of xanthan gum solutions as representative materials for characterizing the mixing. We also studied their rheological properties before mixing using a rheometer (Figure 2). As shown in Figure 2A and B, both sodium alginate and xanthan

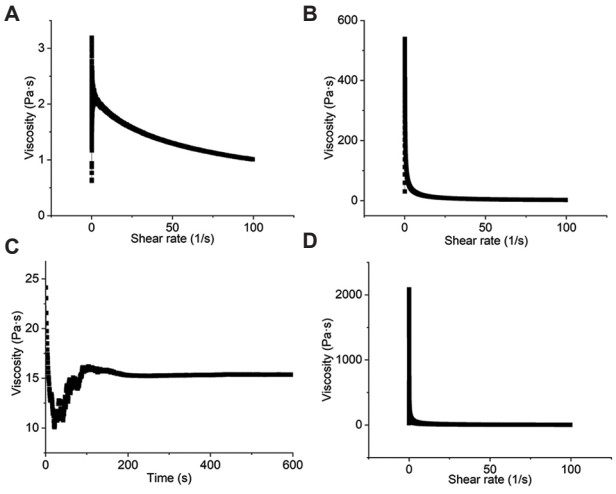


**Figure 2.** Rheological properties of (A) sodium alginate, (B) xanthan gum, (C) their mixture over time, and (D) alginate mixed with $Ca^{2+}$.

gum showed shear-thinning property, but the viscosity of xanthan gum (Figure 2B) is much higher than that of sodium alginate (Figure 2A). Therefore, we can conclude that the viscosity of the mixture also mainly attributes to xanthan gum solution. Moreover, we also performed a time-wise viscosity measurement after the two solutions were mixed. It can be seen that the viscosity remained constant in 10 min, except the initial fluctuation. This is much longer than the mixing time, so we assume that no gelation-induced viscosity change happened during mixing. We also performed flow ramp study for alginate solution mixed with $Ca^{2+}$ and incubated it overnight for full crosslinking (Figure 2D). The result shows that after crosslinking, the viscosity of alginate became much higher, and at 10 1/s shear rate the viscosity of alginate reached 25 Pa·s. This further confirms that during the AAMP mixing, viscosity did not change much due to the crosslinking, while the initial change in Figure 2C might be due to fluctuation as the equipment just started rotating. Figure 3 shows the colorimetric characterization of different mixing conditions. Figure 3A and C shows the mixing results for the gel with and without the alginate/$Ca^{2+}$ reaction, respectively, at varying stages of mixing cycles at a speed of 3000 rpm. In both cases, it was seen that better homogeneity was achieved with increased mixing cycles. The mixing reached visual homogeneity at 50 cycles. These qualitative results were further confirmed by a quantitative analysis using colorimetry (Figure 3B and D). It was seen that the percent variance decreased for both R and B values as mixing cycle number increased. The lighter color of the gels in Figure 3C is probably due to darker color of the initial solution.

We also sought to determine the effect of speed on achieving homogeneity. Hydrogel mixing under 3 different speeds was compared (Figure 3E). Gel without the alginate/$Ca^{2+}$ reaction was used to more easily visualize the difference between the different speeds. The fastest mixing used is 3000 rpm. With all three being mixed for 20 cycles, visually, it was observed that the faster mixing

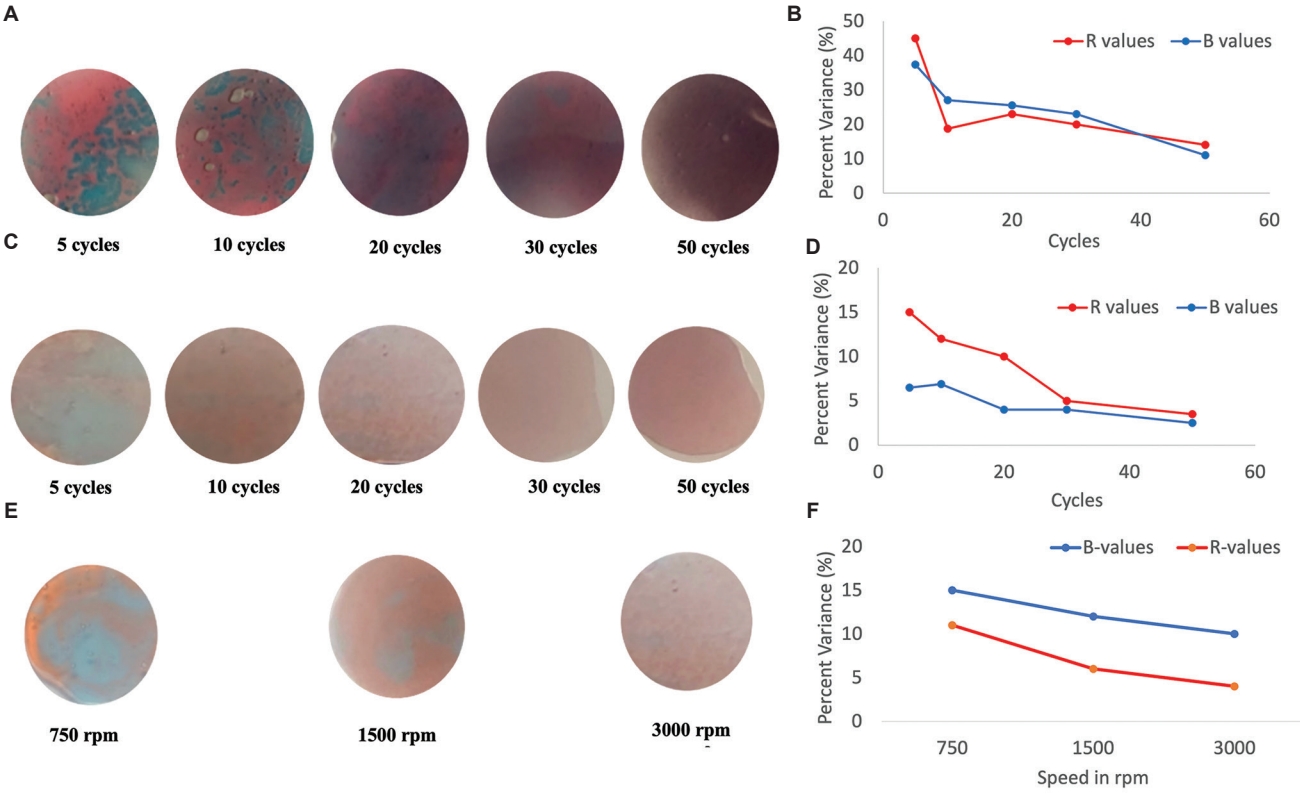


**Figure 3.** Characterization of hydrogel mixing. (A) Hydrogel with $Ca^{2+}$/Alginate reaction mixed by the AAMP at 5, 10, 20, 30, and 50 mixing cycles. (B) Standard deviation/percent variance of red (R) and blue (B) values in the case of 5, 10, 20, 30, and 50 mixing cycles by the dual-syringe mixing device. Values decrease with increased cycle number which demonstrates increased homogeneity with increased mixing. (C) Hydrogel without reaction mixed by the AAMP at 5, 10, 20, 30, and 50 mixing cycles. (D) Percent variances of R and B values in the case of 5, 10, 20, 30, and 50 mix cycles by the dual-syringe mixing device. Values decrease with increased cycle number, which demonstrates increased homogeneity with increased mixing. (E) Hydrogel without reaction mixed by the AAMP that underwent 20 mixing cycles at 3000 rpm, 1500 pm, and 750 pm. (F) Percent variances of R and B values in the case of 750, 1500, and 3000 rpm for 20 mixing cycles by the dual-syringe mixing device. Values decrease with increased cycle number, which demonstrates increased homogeneity with increased mixing.

speed allowed homogeneity to be achieved in fewer cycles. Quantification in Figure 3F using the percent variance of R and B values at three different speeds suggests the same trend. Moreover, we performed additional experiments using 30 mL syringes with other forms of hydrogels, including mixing 2.5% of alginate with 6% of Laponite, and mixing 20% of PEGDMA with 6% of xanthan gum. The results of both hydrogel mixing in Figure S1 show similar trends with the results of Figure 3, suggesting the versatility of the AAMP for a broad range of hydrogel mixture.

### 3.3. COMSOL simulation of the mixing outcome

COMSOL simulation was performed to further validate the AAMP mixing outcome. We assigned the viscosity and diffusion coefficient of each component according to empirical values. We further assume that the AAMP was able to achieve homogeneous mixing fast enough, so the effect of gelation was also negligible. Therefore, the simulation could be simplified to a simple mixing model. As a result, we plotted the fluid speed, pressure, and concentrations at selected time points as shown in Figure 4. It can be seen that there was a dramatic increase in the flow speed at the connector region (Figure 4A), which should contribute to most of the mixing outcome. A representative pressure profile at the same time point also corresponds to the flow rate, where high flow rate leads to high pressure (Figure 4B). The pressure profile has shown that the maximum pressure did not exceed 3 psi, which is safe for cell[28]. Such result provides instructive information for fabricating cell-encapsulating hydrogel bioinks as the pumping speed and force can be customized to limit the maximum pressure and shear stress, which in turn ensures cell viability. Such application associated with cell encapsulation has been very useful and widely applied[29-34].

To directly evaluate the outcome of the mixing, the concentration of xanthan gum was plotted at different time points (Figure 4C-E). Initially, the xanthan gum component was completely loaded in the top syringe; as the mixing cycle increased, it began to mix with the alginate component loaded in the bottom syringe, and the concentration of xanthan gum (C[Gum]) began to distribute across the dual-syringe compartment. The simulation result was visualized in the 3D model. The future study is needed to better characterize the fluid properties of the materials we used, and substitute into the simulation model for precise prediction of the experimental results. Nevertheless, the established model provides a useful tool for experimental design.

### 3.4. Cell viability and proliferation

For tissue engineering applications, cell viability and proliferation are fundamental rubrics for evaluating a bioink. To ensure that the AAMP does not introduce cell damage during bioink preparation, we performed 4-week cell viability and proliferation studies to observe cells' behavior after mixing (Figure 5). To validate that the device is cell-friendly, which works for not only one type of cells, we selected two representative cell types, including mesenchymal stem cells and endothelial cells. To study if prolonged mixing influences cell behavior, three groups with different mixing cycles, including 10, 30, and 50, were tested. Figure 5A shows the live/dead staining results for all groups across 4 weeks. It can be seen that cell viability is above 95% for all groups, indicating that the mixing operation did not introduce any potential damage to cell viability. This was further confirmed by a 4-week proliferation study (Figure 5B and C) by measuring the DNA amount in the sample. According to the results, cell concentration remained almost the same across the 4-week period. Such no reduction in cell number indicates that the mixing procedure by AAMP does not introduce any potential damage to cells over the long-term. On the other hand, no increase in cell number was observed, which is possibly due to high overall gel content, leading to too condensed gel and leaving no room for cells to proliferate. However, this is not the focus of this study, as we just wanted to demonstrate that the mixing procedure has no

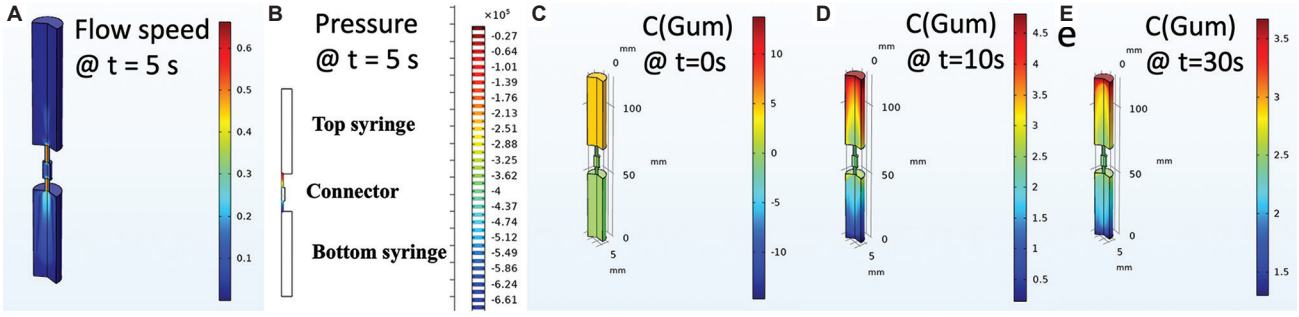


**Figure 4.** COMSOL simulation results for the AAMP mixing process at a frequency of 1 Hz. (A) Flow velocity at t = 5 s. (B) pressure profile at t = 5 s. (C–E) Concentration of the viscosity enhancer, xanthan gum, at t = 0, 10 and 30 s, respectively.

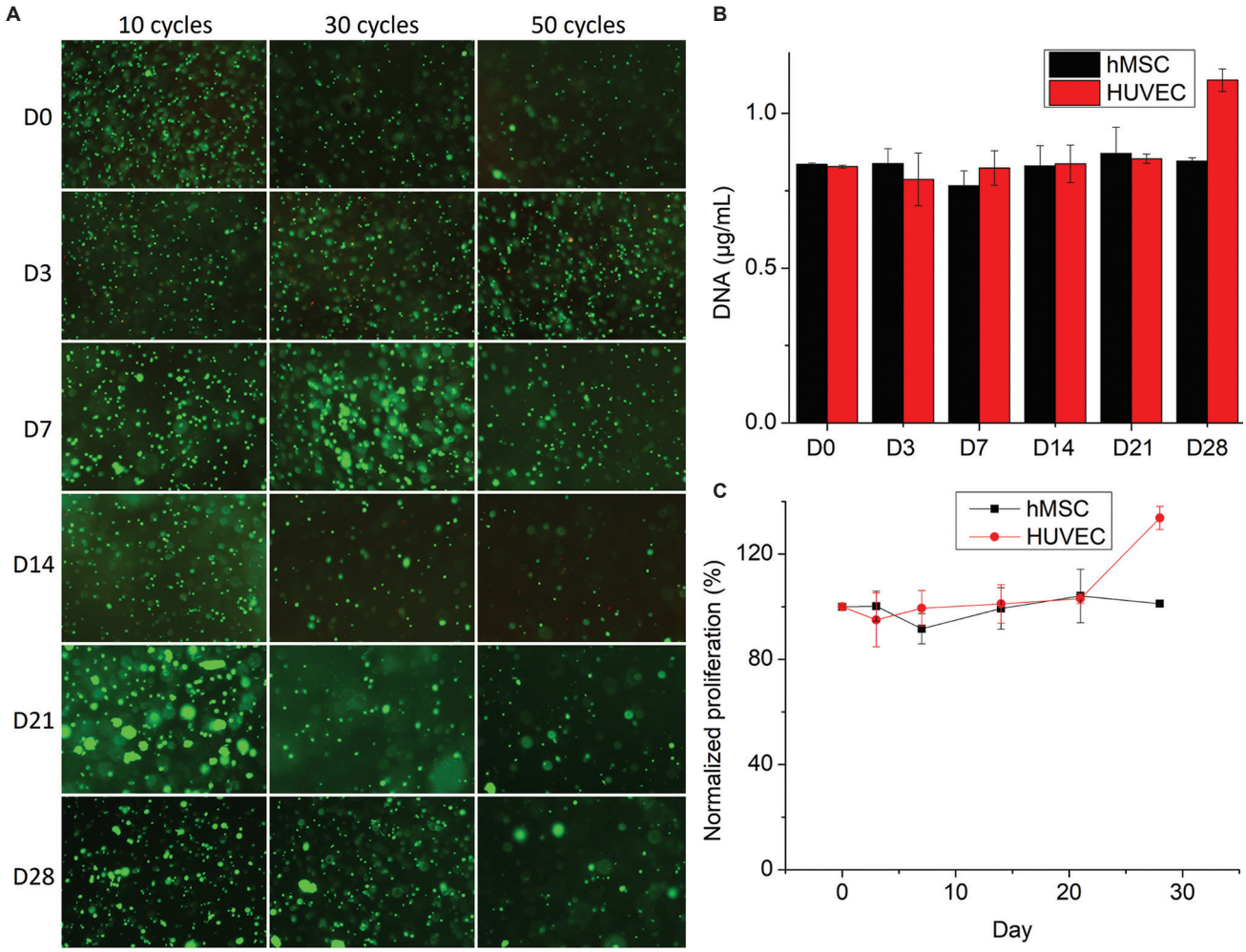


**Figure 5.** Cell viability and proliferation. (A) 4-week viability study for hMSC-laden hydrogels mixed by AAMP for 10, 30, and 50 cycles. (B,C) 4-week proliferation study for hMSC- and HUVEC-laden hydrogels by AAMP for 50 cycles.

negative effect on cell viability. Note that the materials used, including both alginate and xanthan gum, are both known to be non-cytotoxic[35-38], and they were chosen as a general representation of cytocompatible hydrogel components. As the mixing procedure is proven to be cell-friendly, the protocol should work for almost all other commonly seen hydrogel bioink materials, such as gelatin[39-42] and poly(ethylene glycol) diacrylate (PEGDA)[43,44]. Therefore, the AAMP can be a widely applicable platform for preparing cell-laden hydrogel bioink. There is currently little to no literature discussing the outcomes of various methodologies for mixing, with most of the advancement lying in the commercial realm. This is especially concerning given the importance of cell viability and proliferation post-mixing, both which are rarely studied or discussed. Beyond introducing a new mixing device, this study holds the secondary purpose of addressing a foundational gap in research surrounding hydrogel mixing.

## 4. Conclusion

The AAMP provides a mechanism of high pumping frequency and speed that is portable, easily controllable and low-cost compared to those on the market today. Analyses outlined in this paper have shown that the AAMP is an effective means to achieve homogeneity for hydrogels with and without an alginate-$Ca^{2+}$ reaction. By tuning speed and cycle parameters, it was found that by programming the AAMP to complete 50 mixing cycles at 3000 rpm, visual homogeneity was achieved for the hydrogels utilized in our tests, which was further confirmed by colorimetric analysis.

Through the results confirmed by both experiment and simulation, the AAMP is shown to be a cost-effective and efficient adaptation of the traditional manual active mixer that eliminates the need for human labor and the discomfort and error associated with it. Compared with

static mixing that may not achieve uniform mixing if the solutions are too viscous, AAMP ensures the homogeneity of the mixing outcome by limitlessly increasing the number of mixing cycles. Its customizable settings can be built upon and provides a myriad of possibilities for hydrogel quality enhancement. Our results suggest that the AAMP presents great potential for efficient and standardized preparation of hydrogels as well as the field of tissue engineering in general.

## Acknowledgments

This research was partially funded through financial support from NIH grants U01AR069395, R01AR072613, and R01AR074458 from NIAMS, and DoD grant W81XWH-20-1-0343, the Stanford Woods Institute for the Environment, Boswell Foundation, Stanford MCHRI postdoc fellowship, and Tad and Diane Taube Family Foundation.

## Funding

NIH grants U01AR069395, R01AR072613, and R01AR074458 from NIAMS

DoD grant W81XWH-20-1-0343

The Stanford Woods Institute for the Environment

Boswell Foundation

Stanford MCHRI postdoc fellowship

Tad and Diane Taube Family Foundation.

## Conflict of interest

The authors declare that they have no known competing financial interests or personal relationships that could have appeared to influence the work reported in this paper.

## Author contributions

*Conceptualization:* Jiannan Li and Yunzhi Peter Yang
*Investigation:* Jiannan Li, Tara Shelby, Hannah Shelby, and Hossein Vahid Alizadeh
*Formal analysis:* Jiannan Li, Tara Shelby, and Hossein Vahid Alizadeh
*Writing – Original draft:* Jiannan Li, Tara Shelby, and Yunzhi Peter Yang
*Writing – Review and editing:* Jiannan Li, Tara Shelby, Hossein Alizadeh, and Yunzhi Peter Yang.

## Ethics approval and consent to participate

Not applicable.

## Consent for publication

Not applicable.

## Availability of data

Supporting data are available on request. Please contact our research group at peteryanglablist@lists.stanford.edu.

## References

1. Aswathy SH, Narendrakumar U, Manjubala I, 2020, Commercial hydrogels for biomedical applications. *Heliyon*, 6: e03719.

   https://doi.org/10.1016/j.heliyon.2020.e03719

2. Billiet T, Vandenhaute M, Schelfhout J, *et al*., 2012, A review of trends and limitations in hydrogel-rapid prototyping for tissue engineering. *Biomaterials*, 33: 6020–6041.

   https://doi.org/10.1016/j.biomaterials.2012.04.050

3. Khademhosseini A, Langer R, 2007, Microengineered hydrogels for tissue engineering. *Biomaterials*, 28: 5087–5092.

   https://doi.org/10.1016/j.biomaterials.2007.07.021

4. Zhu J, Marchant RE, 2011, Design properties of hydrogel tissue-engineering scaffolds. *Expert Rev Med Devices*, 8: 607–626.

   https://doi.org/10.1586/erd.11.27

5. Ji S, Guvendiren M, 2017, Recent advances in bioink design for 3D bioprinting of tissues and organs. *Front Bioeng Biotechnol*, 5: 23.

   https://doi.org/10.3389/fbioe.2017.00023

6. Jia J, Richards DJ, Pollard S, *et al*., 2014, Engineering alginate as bioink for bioprinting. *Acta Biomater*, 10: 4323–4331.

   https://doi.org/10.1016/j.actbio.2014.06.034

7. Kesti M, Muller M, Becher J, *et al*., 2015, A versatile bioink for three-dimensional printing of cellular scaffolds based on thermally and photo-triggered tandem gelation. *Acta Biomater*, 11: 162–172.

   https://doi.org/10.1016/j.actbio.2014.09.033

8. Kumar H, Sakthivel K, Mohamed MG, *et al*., 2021, Designing gelatin methacryloyl (GelMA)-based bioinks for visible light stereolithographic 3D biofabrication. *Macromol Biosci*, 21: e2000317.

   https://doi.org/10.1002/mabi.202000317

9. Li N, Guo R, Zhang ZJ, 2021, Bioink formulations for bone tissue regeneration. *Front Bioeng Biotechnol*, 9: 630488.

   https://doi.org/10.3389/fbioe.2021.630488

10. Naranda J, Bracic M, Vogrin M, *et al*., 2021, Recent advancements in 3D printing of polysaccharide hydrogels in cartilage tissue engineering. *Materials (Basel)*, 14: 3977.

    https://doi.org/10.3390/ma14143977

11. Possl A, Hartzke D, Schmidts TM, *et al*., 2021, A targeted rheological bioink development guideline and its systematic correlation with printing behavior. *Biofabrication*, 13: 035021.

https://doi.org/10.1088/1758-5090/abde1e

12. Unagolla JM, Jayasuriya AC, 2020, Hydrogel-based 3D bioprinting: A comprehensive review on cell-laden hydrogels, bioink formulations, and future perspectives. *Appl Mater Today*, 18: 100479.

    https://doi.org/10.1016/j.apmt.2019.100479

13. Yin J, Yan M, Wang Y, *et al*., 2018, 3D bioprinting of low-concentration cell-laden gelatin methacrylate (GelMA) bioinks with a two-step cross-linking strategy. *ACS Appl Mater Interfaces*, 10: 6849–6857.

    https://doi.org/10.1021/acsami.7b16059

14. Zheng Z, Wu J, Liu M, *et al*., 2018, 3D bioprinting of self-standing silk-based bioink. *Adv Healthc Mater*, 7: e1701026.

    https://doi.org/10.1002/adhm.201701026

15. Puertas-Bartolome M, Wlodarczyk-Biegun MK, Del Campo A, *et al*., 2020, 3D printing of a reactive hydrogel bio-ink using a static mixing tool. *Polymers (Basel)*, 12: 1986.

    https://doi.org/10.3390/polym12091986

16. Tamayol A, Najafabadi AH, Aliakbarian B, *et al*., 2015, Hydrogel templates for rapid manufacturing of bioactive fibers and 3D constructs. *Adv Healthc Mater*, 4: 2146–2153.

    https://doi.org/10.1002/adhm.201500492

17. Li Y, Yang HY, Lee DS, 2021, Advances in biodegradable and injectable hydrogels for biomedical applications. *J Control Release*, 330: 151–160.

    https://doi.org/10.1016/j.jconrel.2020.12.008

18. Ma T, Lv L, Ouyang C, *et al*., 2021, Rheological behavior and particle alignment of cellulose nanocrystal and its composite hydrogels during 3D printing. *Carbohydr Polyme*, 253: 117217.

    https://doi.org/10.1016/j.carbpol.2020.117217

19. Zhang W, Ma X, Li Y, *et al*., 2020, Preparation of smooth and macroporous hydrogel via hand-held blender for wound healing applications: *In-vitro* and *in-vivo* evaluations. *Biomed Mater*, 15: 055032.

    https://doi.org/10.1088/1748-605X/ab9d6f

20. Mulakkal MC, Trask RS, Ting VP, *et al*., 2018, Responsive cellulose-hydrogel composite ink for 4D printing. *Mater Des*, 160: 108–118.

    https://doi.org/10.1016/j.matdes.2018.09.009

21. Fu YC, Chen CH, Wang CZ, *et al*., 2013, Preparation of porous bioceramics using reverse thermo-responsive hydrogels in combination with rhBMP-2 carriers: *In vitro* and *in vivo* evaluation. *J Mech Behav Biomed Mater*, 27: 64–76.

    https://doi.org/10.1016/j.jmbbm.2013.06.009

22. Müller M, Öztürk E, Arlov Ø, *et al*., 2017, Alginate sulfate-nanocellulose bioinks for cartilage bioprinting applications. *Ann Biomed Eng*, 45: 210–223.

    https://doi.org/10.1007/s10439-016-1704-5

23. Apelgren P, Amoroso M, Säljö K, *et al*., 2018, Skin grafting on 3D bioprinted cartilage constructs *in vivo*. *Plast Reconstr Surg Glob Open*, 6: e1930.

    https://doi.org/10.1097/GOX.0000000000001930

24. Apelgren P, Amoroso M, Lindahl A, *et al*., 2017, Chondrocytes and stem cells in 3D-bioprinted structures create human cartilage *in vivo*. *PLoS One*, 12: e0189428.

    https://doi.org/10.1371/journal.pone.0189428

25. Cohen DL, Lo W, Tsavaris A, *et al*., 2011, Increased mixing improves hydrogel homogeneity and quality of three-dimensional printed constructs. *Tissue Eng Part C Methods*, 17: 239–248.

    https://doi.org/10.1089/ten.TEC.2010.0093

26. Lowe SB, Tan VT, Soeriyadi AH, *et al*., 2014, Synthesis and high-throughput processing of polymeric hydrogels for 3D cell culture. *Bioconjug Chem*, 25: 1581–1601.

    https://doi.org/10.1021/bc500310v

27. Rabanel JM, Hildgen P, 2004, Preparation of hydrogel hollow particles for cell encapsulation by a method of polyester core degradation. *J Microencapsul*, 21: 413–431.

    https://doi.org/10.1080/02652040410001729223

28. Billiet T, Gevaert E, De Schryver T, *et al*., 2014, The 3D printing of gelatin methacrylamide cell-laden tissue-engineered constructs with high cell viability. *Biomaterials*, 35: 49–62.

    https://doi.org/10.1016/j.biomaterials.2013.09.078

29. Wang LH, Ernst AU, An D, *et al*., 2021, A bioinspired scaffold for rapid oxygenation of cell encapsulation systems. *Nat Commun*, 12: 5846.

    https://doi.org/10.1038/s41467-021-26126-w

30. Touani FK, Borie M, Azzi F, *et al*., 2021, Pharmacological preconditioning improves the viability and proangiogenic paracrine function of hydrogel-encapsulated mesenchymal stromal cells. *Stem Cells Int*, 2021: 6663467.

    https://doi.org/10.1155/2021/6663467

31. Pan Z, Bui L, Yadav V, *et al*., 2021, Conformal single cell hydrogel coating with electrically induced tip streaming of an AC cone. *Biomater Sci*, 9: 3284–3292.

    https://doi.org/10.1039/d0bm02100h

32. Karimi S, Bagher Z, Najmoddin N, *et al*., 2021, Alginate-magnetic short nanofibers 3D composite hydrogel enhances the encapsulated human olfactory mucosa stem cells bioactivity for potential nerve regeneration application. *Int J Biol Macromol*, 167: 796–806.

    https://doi.org/10.1016/j.ijbiomac.2020.11.199

33. Hwang DG, Jo Y, Kim M, *et al*., 2021, A 3D bioprinted hybrid encapsulation system for delivery of human pluripotent stem cell-derived pancreatic islet-like aggregates. *Biofabrication*, 14: 014101.

https://doi.org/10.1088/1758-5090/ac23ac

34. Ghasemi A, Akbari E, Imani R, 2021, An overview of engineered hydrogel-based biomaterials for improved β-cell survival and insulin secretion. *Front Bioeng Biotechnol*, 9: 662084.

https://doi.org/10.3389/fbioe.2021.662084

35. Bonani W, Cagol N, Maniglio D, 2020, Alginate hydrogels: A tool for 3D cell encapsulation, tissue engineering, and biofabrication. *Adv Exp Med Biol*, 1250: 49–61.

https://doi.org/10.1007/978-981-15-3262-7_4

36. Garcia-Ochoa F, Santos VE, Casas JA, *et al*., 2000, Xanthan gum: Production, recovery, and properties. *Biotechnol Adv*, 18: 549–579.

https://doi.org/10.1016/s0734-9750(00)00050-1

37. Riaz T, Iqbal MW, Jiang B, *et al*., 2021, A review of the enzymatic, physical, and chemical modification techniques of xanthan gum. *Int J Biol Macromol*, 186: 472–489.

https://doi.org/10.1016/j.ijbiomac.2021.06.196

38. Wang L, Li W, Qin S, 2021, Three polymers from the sea: unique structures, directional modifications, and medical applications. *Polymers (Basel)*, 13: 2482.

https://doi.org/10.3390/polym13152482

39. Van Hoorick J, Tytgat L, Dobos A, *et al*., 2019, (Photo-) crosslinkable gelatin derivatives for biofabrication applications. *Acta Biomater*, 97: 46–73.

https://doi.org/10.1016/j.actbio.2019.07.035

40. Chen H, Fei F, Li X, *et al*., 2021, A structure-supporting, self-healing, and high permeating hydrogel bioink for establishment of diverse homogeneous tissue-like constructs. *Bioact Mater*, 6: 3580–3595.

https://doi.org/10.1016/j.bioactmat.2021.03.019

41. Marques CF, Diogo GS, Pina S, *et al*., 2019, Collagen-based bioinks for hard tissue engineering applications: A comprehensive review. *J Mater Sci Mater Med*, 30: 32.

https://doi.org/10.1007/s10856-019-6234-x

42. Rajabi N, Rezaei A, Kharaziha M, *et al*., 2021, Recent advances on bioprinted gelatin methacrylate-based hydrogels for tissue repair. *Tissue Eng Part A*, 27: 679–702.

https://doi.org/10.1089/ten.TEA.2020.0350

43. Magalhaes LS, Santos FE, de Maria Vaz Elias C, *et al*., 2020, Printing 3D hydrogel structures employing low-cost stereolithography technology. *J Funct Biomater*, 11: 12.

https://doi.org/10.3390/jfb11010012

44. Acosta-Velez GF, Zhu TZ, Linsley CS, *et al*., 2018, Photocurable poly(ethylene glycol) as a bioink for the inkjet 3D pharming of hydrophobic drugs. *Int J Pharm*, 546: 145–153.

https://doi.org/10.1016/j.ijpharm.2018.04.056